Reverse mutational scanning of spike BA.2.86 identifies the epitopes contributing to immune escape from polyclonal sera

Najat Bdeir[1], Tatjana Lüddecke[1], Henrike Maaß[1], Stefan Schmelz[2], Henning Jacobsen[1], Kristin Metzdorf[1], Anne Cossmann[3], Metodi V. Stankov[3], Markus Hoffmann[4,5], Stefan Pöhlmann[4,5], Wulf Blankenfeldt[2,6], Alexandra Dopfner-Jablonka[3,7], Georg M.N. Behrens[3,7,8,#], Luka Čičin-Šain*[1,7,8,#]

[1] Department of Viral Immunology, Helmholtz Centre for Infection Research Braunschweig, Germany

[2] Department Structure and Function of Proteins, Helmholtz Centre for Infection Research Braunschweig, Germany

[3] Department of Rheumatology and Immunology, Hannover Medical School, Hannover, Germany

[4] Infection Biology Unit, German Primate Center – Leibniz Institute for Primate Research, Göttingen, Germany

[5] Faculty of Biology and Psychology, University Göttingen, Göttingen, Germany

[6] Institute for Biochemistry, Biotechnology and Bioinformatics, Technische Universität Braunschweig, Braunschweig, Germany

[7] German Centre for Infection Research (DZIF), partner site Hannover-Braunschweig, Hannover, Germany

[8] Centre for Individualized Infection Medicine, a joint venture of HZI and MHH, Hannover, Germany

shared senior authorship

*For correspondence: Luka Čičin-Šain: Luka.Cicin-Sain@helmholtz-hzi.de

SUMMARY

The recently detected Omicron BA.2.86 lineage contains more than 30 amino acid mutations relative to BA.2. Here, we identify the epitopes driving immune escape of BA.2.86 and its derivative JN.1 (BA.2.86 + S455L) lineage. We investigated the cross-reactive humoral immunity within a cohort of health care workers against Omicron BA.2.86 and JN.1 by employing pseudo-viral mutants. We demonstrate that BA.2.86 and especially JN.1 evaded neutralization by serum antibodies of fully vaccinated individuals. To discern the contribution of individual epitope mutations to immune escape, we constructed a library of 33 BA.2.86 mutants, each of which harbored a single revertant mutation going back to BA.2. This library was used in a reverse mutational scanning approach to define serum neutralization titers against each epitope separately. The mutations within the receptor binding domain (RBD) at position K356T and to a lesser extent the mutations N460K, V483Δ, A484K, and F486P enhanced the immune escape. More surprisingly, the mutation 16insMPLF within the spike N-terminal domain (NTD) and the mutation P621S in S1/S2 significantly contributed to antibody escape of BA.2.86. Upon XBB.1.5 booster vaccination, neutralization titers against JN.1 and BA.2.86 improved relative to all ancestral strains, and the residual immune escape was driven by mutations at positions 16insMPLF, Δ144Y, E544K, P621S, and A484K.

INTRODUCTION

The emergence of new SARS-CoV-2 virus lineages continues to be a critical aspect of the ongoing epidemic viral spread. Among these lineages, BA.2.86, also known as Pirola, has garnered recent attention owing to its significant antigenic shift away from the prevailing XBB sub-lineage (1, 2). The earliest detection of BA.2.86 was in late July 2023 in Denmark (3-5). By mid-august, it had been detected within several countries and WHO had classified it as a variant of interest (4-6). An outbreak of BA.2.86 recorded in the United Kingdom with a high attack rate (86.6%) within an elderly care home demonstrated the transmissibility of this lineage (7). At present, the extent of disease severity exerted by BA.2.86 is unclear, but its derivative sub-variant JN.1 is on track to become the globally dominant SARS-CoV-2 lineage. The viral spike (S) protein mediates SARS-CoV-2 host cell entry through a multistep process. The initial step involves binding of the S protein to angiotensin converting enzyme-2 receptors (ACE2). This engagement is followed by S protein cleavage by host cell proteases, enabling the S protein to drive fusion of the viral envelope with cellular membranes (8). The S1 domain of the S protein entails an N-terminal domain (NTD) with somewhat unclear functions, and the receptor-binding domain (RBD), which directly binds to ACE2 and is the major target for neutralizing antibodies (8-10). The transmembrane S2 domain drives viral fusion with the host cell membrane, which facilitates the release of viral genetic material into the cytoplasm, and therefore plays an important role in infection. BA.2.86 harbors more than 30 mutations relative to BA.2, encompassing 13 mutations in NTD, 14 in the RBD, and 7 within the pre S1/S2 and S2 domain (11). Furthermore, several BA.2.86 descendants have been identified, including BA.2.86.1 (defining mutation ORF1a:K1973R), JN.1 (L455S), JN.2 (ORF1a:Y621C), JN.3 (ORF1a:T2087I), and BA.2.86.2 (ORF7a:E22D)(2).

The alarming number of BA.2.86 spike mutations has prompted several efforts to characterize the antibody immune escape potential of this lineage. Recent studies demonstrate

reduced pseudo-virus neutralization of BA.2.86 and JN.1 in comparison to BA.2 and B.1 strains and that vaccination with the monovalent BNT162b2 XBB.1.5 adapted vaccine significantly enhances neutralization of BA.2.86 pseudo virus by serum antibodies (12-14). However, the contribution of single mutations to the immune escape of BA.2.86 remains unclear. Mutational scanning approaches, where libraries of viruses with single amino acid mutations in the spike protein are compared to the wild-type virus are powerful tools for the identification of epitopes recognized by monoclonal antibodies (15-17), but polyclonal serum antibodies recognize numerous epitopes simultaneously and redundantly. Therefore, mutating one out of 33 epitopes on an ancestral background may only marginally decrease the serum neutralizing activity if some among the remaining 32 epitopes are recognized by independent antibody clones. To overcome this limitation, we cloned a library of 33 reversion mutants on the BA.2.86 background, each harboring a single mutation reverting the position back to the amino acid in BA.2. This approach allowed us to observe a robust increase in neutralizing activity whenever an immunologically relevant epitope was reintroduced in the spike. We tested this library of BA.2.86 mutants against serum samples collected from a cohort of 30 healthcare workers, before and after vaccination with the BNT162b2 XBB.1.5 adapted vaccine. Our data showed that mutations ins16MPLF, K356T, N460K, V483Δ, A484K, F486P and S621P distributed across NTD, RBD, and S1/S2 domains, contribute to the immune escape of BA.2.86. Additionally, we show that vaccination with the BNT162b2 XBB.1.5 adapted vaccine increases substantially the neutralization titers against both BA.2.86 and the more recent BA.2.86.1.1 (JN.1) descendant, and that the immune escape of JN.1 is more pronounced than that of BA.2.86 before, but not after XBB.21.5 booster vaccination. Moreover, we demonstrate that the deletion of the MPLF insertion at position 16, the reinsertion of the tyrosine residue at position 144, as well as the reversions K544E, S621P, and K484A improves neutralization of BA.2.86 upon the XBB.1.5 booster shot.

RESULTS

BA.2.86 spike protein harbors a substantial amount of mutations within all domains

The analysis of the BA.2.86 spike sequence (specifically: hCoV-19/Denmark/DCGC-647694/2023, EPI_ISL_18114953) revealed 33 mutations relative to BA.2 spike (Figure 1). These include 13 mutations within the NTD, 14 mutations in the RBD, and 6 mutations within the S2 and pre S1/S2 domain. Of these mutations, there are five deletions (H69Δ, V70Δ, Y144Δ, N211Δ, and V483Δ) and one insertion after V16 (V16insMPLF). Among mutations that have been previously identified in other variants of interest are R21T (B.1.617), H69Δ/V70Δ (B.1.1.7/Alpha), Y144Δ (XBB1.5; EG.5.1; BA.1), R158G (B.1.617.2/Delta), E484K (B.1.351/Beta; P.1/Gamma) and P681R (B.1.617.2/Delta). Additionally, BA.2.86 harbors several mutations, which were rarely reported (V445H, N450D, N481K, V483Δ; and E554K) (18-20). Among these mutations ins16MPLF, ΔY144, F157S, R158G, H245N, A264D are located within the NTD antigenic supersite and may contribute to immune escape (21). Additionally, several mutations within the RBD of BA.2.86 have been associated with antibody resistance including K356T, A484K, and N450D (9, 22, 23), while several other mutations R493Q, F486P, N460K, and V483Δ may alter ACE2 interactions (24, 25). Hence, BA.2.86 contains a plethora of mutations within the spike protein, which may alter key properties of this virus in receptor binding and neutralizing antibody escape. To visualize the position of mutations in the spike protein of BA.2.86 with respect to BA.2, we used AlphaFold2/AlphaFold-Multimer (26, 27) to construct a structural model of the spike trimer of BA.2.86. The model, which was obtained in a closed state with respect to the conformation of the RBD, shows that mutations with respect to BA.2 are spread over the distal part of the protein but otherwise do not cluster at specific positions (Fig. 1B-C).

BA.2.86 and JN.1 efficiently escape antibody neutralization

To assess the immune escape of the BA.2.86 and BA.2.86.1.1 (JN.1) lineages, we employed pseudo-virus particles (pp) in neutralization assays. For comparison, we also included particles harboring the spike protein of XBB.1.5 ($XBB.1.5_{pp}$), Wuhan-Hu-01 (WT_{pp}), BA.1 ($BA.1_{pp}$), and BA.2 ($BA.2_{pp}$) (Figure 2A-B). We found that plasma obtained from a cohort of at least double boostered individuals neutralized $BA.1_{pp}$ and $BA.2_{pp}$ with 2-fold and 3-fold reduced efficiency as compared to the index $WT_{pp,}$ respectively. However, the inhibition of $BA.2.86_{pp}$ and $XBB.1.5_{pp}$ was 40- and 30-fold reduced, respectively (Figure 2A). Antibody escape of $JN.1_{pp}$ was even more pronounced, with an ~80-fold reduction relative to WT_{pp} (Figure 2A). Plasma acquired post vaccination with the XBB.1.5-adapted mRNA vaccine neutralized $XBB.1.5_{pp}$, $BA.2.86_{pp}$, and $JN.1_{pp}$ with almost comparable efficiency, whereby the mean neutralization titer was 6-fold, 11-fold, and 12-fold lower than WT_{pp}, respectively (Figure 2B). Collectively, BA.2.86 and JN.1 escaped neutralization by antibodies induced upon primary vaccination series and boosters with immunogens predating XBB lineages, whereby this escape was more pronounced in JN.1. However, a vaccination with the XBB.1.5 adapted vaccine boosted the neutralizing titers against both variants to similar extents, reduced the gap in neutralization efficiency between them and Omicron BA.2, and eliminated it completely between JN.1 and BA.2.86.

Mutations ins16MPLF, K356T, N460K, V483Δ, A484K, F486P, and P621S contribute to BA.2.86 neutralizing antibody escape.

To investigate the effect of individual mutations within BA.2.86 on post-vaccination neutralizing antibody escape, we cloned a comprehensive library of 33 individual BA.2.86 mutants. Each of them contains a single reversion relative to the amino acid sequence of BA.2, while retaining the rest of the sequence as in BA.2.86. Geometric means of pseudo-virus

144 neutralization titers (PVNT50) against BA.2.86$_{pp}$ were ~18-fold lower than against BA.2$_{pp}$ prior
145 to vaccination with the XBB.1.5 vaccine (Figure 3A). Hence, we tested which mutations
146 decreased the gap between neutralization of BA.2$_{pp}$ and BA.2.86$_{pp}$. Our data showed that
147 among the BA.2.86$_{pp}$ mutants with single mutations within the NTD, only the insMPLF16Δ$_{pp}$
148 reduced the gap to BA.2$_{pp}$ to a mere 4-fold reduction (Figure 3A). The remaining NTD$_{pp}$ single
149 mutants did not significantly contribute to neutralizing antibody escape, because their
150 neutralization titers were comparable to that of BA.2.86$_{pp}$ (Figure 3B). While the N-terminus
151 of BA.2.86 spike protein is modelled with lesser confidence than the core of the structure
152 (Figure S1A-C), it is interesting that the N-terminal 16MPLF insertion is predicted to interact
153 with a crevice in the N-terminal domain (NTD; Figure S1B-C). This is reminiscent of SARS-
154 CoV spike protein (28), albeit here, the N-terminus is yet more extended and anchored via a
155 disulfide bridge to the core of the NTD (Figure S1D).

156 The neutralization capacity of serum samples against epitopes in the RBD of BA.2.86$_{pp}$ was
157 significantly affected prior to the XBB.1.5 booster by the mutation K356T, which was ~3-fold
158 more efficiently neutralized than BA.2.86$_{pp}$ (Figure 4A and 4B). Additionally, our results
159 showed that K460N$_{pp}$, ΔV483$_{pp}$, K484A$_{pp}$, and P486F$_{pp}$ had a 7-, 8- ,8-, and 10-fold reduced
160 neutralization efficiency, respectively, relative to BA.2$_{pp,}$ and thus much less than the 18-fold
161 reduction observed in BA.2.86$_{pp}$. While the latter results did not raise to statistical significance
162 over BA.2.86$_{pp}$ (Fig. 4B), they indicated an improved neutralization in the presence of these
163 parental epitopes. In contrast, the remaining mutations within the RBD of BA.2.86 did not
164 enhance serum neutralization capacity.

165 In addition to the aforementioned RBD and NTD BA.2.86 mutants, we explored the
166 contribution of mutations within the S1/S2 and S2 regions to antibody evasion. We report a
167 significant increase in neutralization efficiency for BA.2.86 S621P$_{pp}$, whereby neutralization
168 efficiency of BA.2.86 S621P$_{pp.}$ was 3-fold lower than that of BA.2$_{pp}$ and hence, significantly

higher than for BA.2.86$_{pp}$ (Figure 5A and 5B) In contrast, BA.2.86 K554E$_{pp}$, V570A$_{pp}$, R681H$_{pp}$, F939S$_{pp}$, L1143P$_{pp}$ all showed comparable neutralization sensitivity as compared to BA.2.86$_{pp}$ (Figure 5A, and 5B).

Interestingly, the impact of NTD mutations on neutralization escape following vaccination with the adapted XBB.1.5 immunogen revealed that the mutants where the MPLF insertion at position 16 was removed (insMPLF16Δ$_{pp}$), or the reinsertion of the of the Y at position 144 (ins144Y$_{pp}$) recovered the neutralization efficiency of plasma samples to the level of BA.2 neutralization (Figure 6). A similar effect was observed for BA.2.86 mutants K554E$_{pp}$ and K484A$_{pp}$, which demonstrate neutralization efficiency comparable to BA.2$_{pp}$ after XBB.1.5 booster vaccination. On the other hand, the neutralization of the BA.2.86 mutant S621P$_{pp}$ was not significantly increased after the XBB.1.5 booster vaccination (Figure 6). Since neutralization efficiencies of BA.2.86$_{pp}$ and JN.1$_{pp}$ were comparable after the XBB.1.5 booster vaccination, our data may argue that these positions are relevant for the residual immune escape of JN.1 upon the XBB.1.5 booster as well.

Discussion

This work provides to our knowledge the first example of a reverse mutational scanning strategy for the identification of epitopes that contribute to immune escape from vaccine-induced immunity. Strategies based on mutational scanning of the SARS-CoV-2 spike are not new. Others and us have shown that such approaches can be used to generate libraries containing individual mutations present in the Omicron, but not in the ancestral variants, and thus identify epitopes that escape recognition by monoclonal antibodies (16, 17) and polyclonal sera (15, 16, 29). A very comprehensive mutational scanning based on the XBB.1.5 spike has been recently performed by the Bloom lab to introduce 9000 theoretical mutations on the XBB.1.5 background and thus predict future potential escape mutations (15). However, forward mutational scanning cannot predict the emergence of lineages with big evolutionary

194 jumps, such as the Omicron BA.1 and BA.2.86 variants, where more than 30 mutations were
195 observed simultaneously, with no intermittent stages that are known. Moreover, such
196 approaches are not ideal for the analysis of neutralizing potential of polyclonal sera, where
197 redundant epitope recognition may result in virus neutralization even if immunologically
198 relevant epitopes are mutated. By reverse mutational scanning, we provide here a loss-of-
199 function genetic approach, allowing the identification of escape epitopes in polyclonal
200 responses to antigens with many simultaneous mutations. Thus, we identified a collection of
201 epitopes that contribute to immune escape from vaccine-induced immunity by BA.2.86 and its
202 derivative JN.1 lineage. This approach may also be rapidly deployed for subsequent lineages
203 with big evolutionary jumps that may emerge in the future.
204 The emergence of BA.2.86 harboring more than 30 mutations relative to BA.2 was reminiscent
205 of the Omicron appearance in 2021 and raised concerns regarding its antibody escape potential
206 (12, 13, 30). A number of these mutations (K356, V445, G446, N450, L452, and P621) were
207 also observed in omicron sub-lineages within immunocompromised patients. This may indicate
208 that reduced immune functions within some individuals may be a source of highly mutated
209 SARS-CoV2 lineages (31, 32). BA.2.86 has also evolved several descendants including JN.1
210 which harbors three mutations in non S-proteins and a hallmark S455L mutation in the spike
211 protein (2). In sera from a cohort that was at least double boostered, we observed that the S455L
212 mutation reduces the neutralization efficiency relative to BA.2.86 by a factor of ~2, but that
213 the XBB.1.5 adapted vaccine booster increases neutralization efficiency against both lineages
214 to similar levels, which were merely 2-fold lower than the neutralization of Omicron XBB.1.5.
215 Nevertheless, their neutralization titers remain 5-6 fold lower than that of BA.2 following
216 vaccination, in line with data reported in Stankov et al. (33) and Wang et al. (13).
217 Several mutations within BA.2.86 significantly increased the neutralizing antibody escape
218 prior to vaccination with the adapted XBB.1.5 vaccine. We found that the NTD mutation

ins16MPLF significantly affected neutralization sensitivity, and its reversion resulted in a 4-fold increase in neutralization titers relative to BA.2.86. While this region of the NTD is disordered in published structures of the SARS-CoV-2 spike protein, indicating high intrinsic flexibility, the MPLF insertion is somewhat reminiscent of the SARS-CoV spike protein, where the N-terminus is yet more extended and anchored via a disulfide bridge to the core of the NTD (Fig. S1D). It should be noted that several NTD-binding neutralizing antibodies have been identified in the past (34, 35), indicating that mutations in this domain may indeed interfere with the immune system's capacity to recognize the virus. Even more interestingly, we show that the deletion of the MPLF insertion at position 16 or reinsertion of Y at position 144 increases neutralization efficiency after the adapted XBB.1.5 vaccination to BA.2 levels. Both mutations are located within the NTD antigenic supersite, which is a key target for NTD specific neutralizing antibodies (21). Moreover, in silico structural modeling of BA.2.86 performed by Colson et al. indicates that the MPLF insertion may mask a V-shaped electronegative zone within the NTD, which is an unprecedented phenotype in SARS-CoV-2. This zone may stabilize the virus onto target cells and may induce some long-range conformational changes which affect the RBD with potential consequences on RBD-ACE2 interactions (36). However, our independent in silico analysis of this region of the NTD structure argues that the changes at the N-terminal tip cannot be predicted with a high degree of confidence. Therefore, the actual effects of this mutation on the NTD structure may only be confirmed by empirical analysis in cryoelectron microscopy or similar approaches.

We also found that the mutation K356T within the RBD plays a contributing role to BA.2.86 escape of neutralization by polyclonal sera. This reduction in neutralization efficiency might be attributed to the steric hindrance caused by the introduction of an additional glycosylation site (37). Similarly, we demonstrate that mutations N460K, V483Δ, A484K, and F486P within the RBD enhance neutralizing antibody escape. This is in line with reports from Wang et al,

which show that mutation N460K and F486P shared in XBB.1.5 and EG.5.1 cause resistance to class 1 and 2 monoclonal antibodies (mAb) (38). Structural modelling has shown that the mutation N460K, which was first identified in BA.2.75, disrupts a hydrogen bond formed between the RBD and a class 1 mAb (VH3-53) (39) and a study by Wang et al. demonstrated that the mutation A484K within BA.2.86 reduced the neutralizing activity of a subset of class 3 mAbs (13). The mutation V483Δ has seldom been reported in circulating strains. Full spike mutational scanning of BA.2.86 postulated that V483Δ may contribute to antibody escape but experimental evidence for this has been lacking (15). Our data argue that such effects may be present, albeit not very pronounced. We also show that the mutation P621S in the S1/S2 domain of BA.2.86 contributed to significant neutralization escape and this phenotype, to our knowledge has not been demonstrated previously. In sum, we have identified several mutations that have significantly contributed to immune escape in our cohort. However, we cannot exclude that additional mutations may result in immune escape in individuals whose repertoire differs from our cohort of double boostered individuals. This requires additional studies in cohorts of elderly people or those with immune deficiencies.

In sum, BA.2.86 and its JN.1 descendent efficiently escape neutralization by polyclonal serum antibodies of double boostered individuals, and our data argue that this is due to mutations at positions N460K, V483Δ, A484K, F486P, K356T, P621S, and ins16MPLF. We also observed that the S455N mutation provides a 2-fold increase in neutralization titres over BA.2.86. However, neutralization titres of JN.1 and BA.2.86 were appreciably improved by the XBB.1.5 vaccine booster to comparable levels. This may argue that the JN.1 lineage would have no selective immunological advantage over BA.2.86 in an XBB.1.5-boostered population, and that the residual immune escape of both lineages may rely on the shared epitopes at positions ins16MPLF, Δ144Y, E544K, P621S, and A484K.

Limitations of the Study

We have utilized the well-established pseudo-virus system to assess the contribution of single mutations to the antibody escape potential of BA.2.86. While formal verification would require the use of authentic SARS-CoV-2 with spike mutations introduced by reverse genetics, neutralization titers in pseudo-viral and authentic virus setups have been shown to be comparable due to the immunodominance of spike over other structural elements (40-42). An additional limitation in our study is the lack of information regarding hybrid immunity within our cohort, whereby some participants may have experienced a prior unrecorded infection with XBB sublineages, which may have elicited a humoral immune response similar to vaccination. However, only 4 individuals have a recorded infection in 2023, when the XBB.1.5 lineage was present at high levels. Furthermore, the neutralization sensitivity of BA2.86 and BA.2.86 mutant viruses may vary due to the heterogeneity of immune background within our cohort and maybe distinct to cohorts outside the scope of our present study, including elderly or immunocompromised individuals. An additional limitation is that we have only analyzed a library of single mutants and have not explored the impact of combinations of spike protein mutations on serum neutralization.

AUTHOR CONTRIBUTIONS

Conceptualization: L.C-S.; Methodology: L.C-S; N.B; Investigation: N.B, T.L, H.M, K.M, H.J, S.S; Formal analysis: N.B, S.S, W.B, L.C-S; Resources: S.P., M.H., A.D-J., and G.M.N.B; Funding acquisition: L.C-S; Writing – original draft: N.B.; Writing – review & editing: all authors.

ACKNOWLEDGEMENTS:

This research was funded by the Helmholtz Association through Helmholtz Campaign COVIPA (KA1-Co-02) to L.C-S. and EU-Partnering grant MCMVaccine (PIE-008) to L.C-S.

and S.P. Funding to L.C-S and S.P. was also provided by the Ministry of Science and Culture of Lower Saxony, through the COFONI Network, flex fund projects 6FF22 and 10FF22. G.M.N.B. and A.D.-J. acknowledge funding from Ministry of Science and Culture of Lower Saxony (14-76103-184, COFONI Network, project 4LZF23), G.M.N.B. acknowledges funding by the European Regional Development Fund (ZW7-85151373), and A.D.-J. acknowledge funding by European Social Fund (ZAM5-87006761).

We thank Ayse Barut, Yuliia Polianska, Inge Hollatz-Rangosch and Karina Watzke for expert technical assistance, Natascha Gödecke for support with biosafety compliance and Gert Zimmer (Institute of Virology and Immunology, Mittelhäusern, Switzerland) for providing the VSV pseudo-virus system. We also thank the CoCo Study participants for their support and the entire CoCo study team, especially Annika Heidemann and Luis Manthey, for technical and logistical support.

DECLARATION OF INTERESTS

L.C-S. served as an advisor to Sanofi unrelated to this work. G.M.N.B. served as advisor for Moderna unrelated to this work, A.D-J served as an advisor for Pfizer unrelated to this work, S.P. and M.H. conducted contract research (testing of vaccinee sera for neutralizing activity against SARS-CoV-2) for Valneva unrelated to this work. S.P. served as advisor for BioNTech, unrelated to this work. H.J. served as advisor on COVID neutralization assays for WHO and CEPI, unrelated to this work. The other authors declare no competing interests.

316 **Key Resources table**

317 **Table 1: Bacterial and virus strains**

Bacteria or virus	Source	Catalogue number (N/A=not applicable)
VSV*ΔG-Fluc	Laboratory of Gert Zimmer	N/A
NEB® 10-beta Competent *E. coli*	New England BioLabs	C3019H

318

319 **Table 2: Experimental Models- Cell lines**

Cell line	Source	Catalogue number (N/A=not applicable)
293T	DSMZ	Cat# ACC-635; RRID: CVCL_0063
Vero76	ATCC	Cat# CRL-1586

320

321 **Table 3: Oligonucleotides**

Oligos	Source	Catalogue number (N/A=not applicable)
SARS-2--S (D264A) F (gctTACTATGTGGGCTACCTGC)	Sigma-Aldrich	N/A
SARS-2--S (D264A) R (GGCGGCACCAGCTG)	Sigma-Aldrich	N/A
SARS-2-S (V570A) F (gccGATACCACAGACGCC)	Sigma-Aldrich	N/A
SARS-2-S (V570A) R (GATATCCCGGCCAAAC)	Sigma-Aldrich	N/A
SARS-2-S (K554E) F (gagAGCAACAAGAAGTTCCTGC)	Sigma-Aldrich	N/A
SARS-2-S (K554E) R (TGTCAGCACGCCGG)	Sigma-Aldrich	N/A
SARS-2-S (P486F) F (ttcAACTGCTACTTCCCAC)	Sigma-Aldrich	N/A
SARS-2-S (P486F) R (GCCCTTGCCCTTAC)	Sigma-Aldrich	N/A
SARS-2-S (H339G) F (ggcGAGGTGTTCAATGCC)	Sigma-Aldrich	N/A
SARS-2-S (H339G) R (GAAG	Sigma-Aldrich	N/A
SARS-2-S (S446G) F (ggcGGCAACTACGATTACTG)	Sigma-Aldrich	N/A
SARS-2-S (S446G) R (GTGTTTGGAGTCCAG)	Sigma-Aldrich	N/A

SARS-2-S (N245H) F (cacAGAAGCTACCTGACACC)	Sigma-Aldrich	N/A
SARS-2-S (N245H) R (CAGGGCCAGCAGTG)	Sigma-Aldrich	N/A
SARS-2-S (V332I) F (atcACCAATCTGTGCCC)	Sigma-Aldrich	N/A
SARS-2-S (V332I) R (ATTGGGGAACCGCAC)	Sigma-Aldrich	N/A
SARS-2-S (Δ insMPLF) F (ACCTGATCACAACAAC)	Sigma-Aldrich	N/A
SARS-2-S (Δ insMPLF) R (TCACACACTGGCTG)	Sigma-Aldrich	N/A
SARS-2-S (T356K) F (aagCGGATCAGCAATTGCG)	Sigma-Aldrich	N/A
SARS-2-S (T356K) R (CCGGTTCCAGGCGTAC)	Sigma-Aldrich	N/A
SARS-2-S (I212L) F (CACCCCTATCctgGGGCGGGATT)	Sigma-Aldrich	N/A
SARS-2-S (I212L) R (TGCTTGCTGTAGATCTTGAAG)	Sigma-Aldrich	N/A
SARS-2-S (F216L) F (ctgCCTCAGGGCTTCTCTG)	Sigma-Aldrich	N/A
SARS-2-S (F216L) R (ATCCCGCCCGATGATAG)	Sigma-Aldrich	N/A
SARS-2-S (W452L) F (ttgTACCGGCTGTTCCG)	Sigma-Aldrich	N/A
SARS-2-S (W452L) R (GTAATCGTAGTTGCCG)	Sigma-Aldrich	N/A
SARS-2-S (insN211) F (accTCGgGCGGGATttcc)	Sigma-Aldrich	N/A
SARS-2-S (insN211) R (tGATAGGGGTGTGCTTG)	Sigma-Aldrich	N/A
SARS-2-S (D450N) F (aatTACTGGTACCGGCTG)	Sigma-Aldrich	N/A
SARS-2-S (D450N) R (GTAGTTGCCGCTGTG)	Sigma-Aldrich	N/A
SARS-2-S (K460N) F (aacCTGAAGCCCTTCGAG)	Sigma-Aldrich	N/A
SARS-2-S (K460N) R (GGACTTCCGGAACAG)	Sigma-Aldrich	N/A
SARS-2-S (K481N) F (aacGGCAAGGGCCCCAAC)	Sigma-Aldrich	N/A
SARS-2-S (K481N) R (ACAAGGCTTGTTGCCG)	Sigma-Aldrich	N/A
SARS-2-S (S621P) F (cccGTGGCCATTCACGC)	Sigma-Aldrich	N/A
SARS-2-S (S621P) R (CACTTCGGTACAGTTCAC)	Sigma-Aldrich	N/A

SARS-2-S (L1143P) F (cccGAGCTGGACAGCTTC)	Sigma-Aldrich	N/A
SARS-2-S (L1143P) R (CTGCAGAGGGTCGTAC)	Sigma-Aldrich	N/A
SARS-2-S (Q493R) F (cggTCCTACGGCTTTCG)	Sigma-Aldrich	N/A
SARS-2-S (Q493R) R (CAGTGGGAAGTAGCAG)	Sigma-Aldrich	N/A
SARS-2-S (T21R) F (cgcACCCAGTCCTACAC	Sigma-Aldrich	N/A
SARS-2-S (T21R) R (TGTGATCAGGTTGAACAG)	Sigma-Aldrich	N/A
SARS-2-S (G158R) F (cggGTGTACAGCAGCGC)	Sigma-Aldrich	N/A
SARS-2-S (K158R) R (GGACTCGCTTTCCATC)	Sigma-Aldrich	N/A
SARS-2-S (K403R) F (aggGGAAATGAAGTGAGCC)	Sigma-Aldrich	N/A
SARS-2-S (K403R) R (GATCACGAAGCTGTC)	Sigma-Aldrich	N/A
SARS-2-S (L50S) F (agcACCCAGGACCTGTTC)	Sigma-Aldrich	N/A
SARS-2-S (L50S) R (GTGCAGCACGCTGG)	Sigma-Aldrich	N/A
SARS-2-S (F939S) F (ccAGCACAGCAAGCGC)	Sigma-Aldrich	N/A
SARS-2-S (F939S) F (CAGGCTGTCCTGGATC)	Sigma-Aldrich	N/A
SARS-2-S (L125V) F (gtCATCAAAGTGTGCGAGTTCC)	Sigma-Aldrich	N/A
SARS-2-S (L125V) F (CACGTTGGTGGCGTTG)	Sigma-Aldrich	N/A
SARS-2-S (H445V) F (gtcAGCGGCAACTACGATTAC)	Sigma-Aldrich	N/A
SARS-2-S (H445V) R (TTTGGAGTCCAGCTTG)	Sigma-Aldrich	N/A
SARS-2-S (S157F) F (ttcGGGGTGTACAGCAG)	Sigma-Aldrich	N/A
SARS-2-S (S157F) R (CTCGCTTTCCATCC)	Sigma-Aldrich	N/A
SARS-2-S (insH69) F (cactCCGGCACCAATG)	Sigma-Aldrich	N/A
SARS-2-S (insH69) R (GATGGCGTGGAACCAg)	Sigma-Aldrich	N/A
SARS-2-S (insH70) F (gtctCCGGCACCAATG)	Sigma-Aldrich	N/A
SARS-2-S (insH70) R (GATGGCGTGGAACCAg)	Sigma-Aldrich	N/A

SARS-2-S JN.1 F (CTGGTACCGGagcTTCCGGAAGTC)	Sigma-Aldrich	N/A
SARS-2-S JN.1 R (TAATCGTAGTTGCCG)	Sigma-Aldrich	N/A

Table 4: Recombinant DNA

Recombinant DNA	Source	Catalogue number (N/A=not applicable)
pCAGGS-DsRed	Laboratory of Stefan Pöhlmann	N/A
pCG1-SARS-2-SΔ18 BA.2.86	Laboratory of Stefan Pöhlmann	N/A
pCG1-SARS-2-SΔ18 BA.2.86 S446G	Laboratory of Stefan Pöhlmann	N/A
pCG1-SARS-2-SΔ18 BA.2.86 F939S	Laboratory of Stefan Pöhlmann	N/A
pCG1-SARS-2-SΔ18 BA.2.86 Δ483Y	Laboratory of Stefan Pöhlmann	N/A
pCG1-SARS-2-SΔ18 BA.2.86 Δ144Y	Laboratory of Stefan Pöhlmann	N/A
pCG1-SARS-2-SΔ18 BA.2.86 K484A	Laboratory of Stefan Pöhlmann	N/A
pCG1-SARS-2-SΔ18 BA.2.86 R681H	Laboratory of Stefan Pöhlmann	N/A
Remaining pCG1-SARS-2-SΔ18 (BA2.86) single point mutants	Laboratory of Luka Cicin-Sain	N/A

Table 5: Software and algorithms

Software	Source	Version number
GraphPad Prism	GraphPad Software	9.0
Microsoft Office Standard	Microsoft Corporation	2010

Materials and Methods

Cell lines

All cell lines were maintained at 37 °C and 5% CO_2 in a humified environment. 293T (Human, kidney) and VeroE6 (African green monkey, kidney) cells were cultured in Dulbecco's Modified Eagle Medium (DMEM, ThermoFisher Scientific) supplemented with 5% fetal bovine serum (FBS, ThermoFisher Scientific) and 100 U/ml penicillin and 0.1 mg/ml Streptomycin (PAN-Biotec). Both cell lines were used to a maximum passage of 30. For seeding and sub-cultivation, cells were washed with phosphate buffered saline (PBS, PAN-

Biotec) and then incubated with trypsin/EDTA (PAN-Biotec) until cell detachment. Cell lines were routinely tested for mycoplasma. Transfection of 293T cells for the production of pseudoviruses was carried out by calcium phosphate transfection.

Plasmids

The plasmid pCG1_SARS-2-Sdel18 (Codon-optimized) encoding the spike protein of the Wuhan-Hu-1 SARS-CoV-2 has been previously reported (8). The pCG1_SARS-2-Sdel18 BA.1 and BA.2 expression plasmids are previously reported (29) and based on isolate hCoV-19/Botswana/R40B58_BHP_3321001245/2021 (GISAID Accession ID: EPI_ISL_6640919) and isolate hCoV-19/England/PHEC-4G0AFZF7/2021 (GISAID Accession ID: EPI_ISL_8738174) respectively. The pCG1_SARS-2-Sdel18 XBB expression plasmid was generated by Gibson assembly based on the expression vector for the spike of Omicron BA.2 and site directed mutagenesis was done to generate XBB.1.5. Expression plasmids pCAGGS-DsRed and pCG1-SARS-2-SDel18 BA.2.86 (based on the isolate hCoV-19/Denmark/DCGC-647694/2023, EPI_ISL_18114953) were kindly provided by the Laboratory of Stefan Pöhlmann. Site directed mutagenesis (Q5® High-Fidelity 2X Master Mix, New England BioLabs) was utilized for the generation of the SARS-CoV-2 spike BA.2.86 expression plasmid library containing single point mutations back to BA.2 spike. Primers are listed in Table 3.

Production of Pseudo-viruses and titration

Production of pseudo-viruses was performed according to published protocol (43). In brief, 293T cells were seeded in 6 well plates at a confluency of 70%. The next day, cells were transfected with expression plasmids for pCG1-SARS-2-SΔ18 WT, pCG1-SARS-2-SΔ18 BA2.86, pCG1-SARS-2-SΔ18 BA2, pCG1-SARS-2-SΔ18 BA2.86 XBB or pCG1-SARS-2-SΔ18 BA2.86 single point mutants. At 24 hours post transfection, cells were incubated for 1 hour with a replication deficient VSV (VSV*ΔG) expressing enhanced

green fluorescent protein (eGFP) and firefly luciferase at an MOI of 3. Subsequently, cells were washed with phosphate buffered saline (PBS) and incubated with anti-VSV-G antibody (mouse hybridoma supernatant from CRL-2700; ATCC) in order to neutralize residual input virus. At 12 hours post infection, supernatants were harvested and cleared from cell debris by centrifugation and stored at -80C for later use. All pseudo-viruses were titrated on VeroE6 confluent 96 well plates to ensure comparable infectivity according to a previously published protocol (29).

Neutralization assay

Neutralization assays were based on a previously published protocol (29). All plasma samples utilized in this study were heat inactivated at 56 °C for 30 minutes and stored at 4 °C for further use. Pseudo-viral particles (600pfu/well± 30%) were incubated for one hour in a 96 well microtiter plate with two-fold diluted serum samples in DMEM [1% Penicillin-Streptomycin, 1% L-Glu, 5% FBS] ranging from 1:10 to 1:5120. Pseudo-virus particles were incubated in the absence of sera as controls indicating 0% inhibition. After incubation, the serum/virus samples were transferred onto a confluent VeroE6 96 well plate. After a 24-hour incubation, plates were fixed with 4% paraformaldehyde (PFA) and stored at 4 °C until readout. GFP+ infected cells were counted using an IncuCyte S3 (Sartorius) performing whole-well scans (4x) in phase contrast and green fluorescence settings (300ms exposure). Automated segmentation and counting of fluorescent foci defined as green fluorescent protein GFP+-single cells was performed using the IncuCyte GUI software (versions 2019B Rev1 and 2021B). Pseudo-virus neutralization titer 50 (PVNT50) values were determined by a non-linear regression model. The lower limit of confidence (LLOC) was set at a PVNT50 of 6.25 (dashed line). Non-responders are defined as individuals below this threshold. All PVNT50 below 1 are set at 1 for visualization purposes. Due to technical limitations, sample numbers in our assays were randomly distributed to have at least 20 individual sera within each group.

Ethics committee Approval

The collection of all plasma samples was approved by the research ethics committee of the Institutional Review Board of Hannover Medical School (8973 BO K 2020). All donors provided written consent for the blood donation and use for research purposes.

Plasma Samples

The number of participants within this analysis is n=30. Median age is 45 years (interquartile range (IQR) 33 to 56.25) and mean age is 46 (SD=12.23). Male to female ratio is 1:3. Among these participants, 30% were vaccinated with 3 vaccine doses, 63.3% were vaccinated with four vaccine doses, and 6.6% were vaccinated with more than four doses. Ten participants (33,3%) were vaccinated with the bivalent WT/BA.4/5 vaccine. The median time in months since last recorded SARS-CoV-2 infection for the patients with known infection is 14.5 (IQR 10.75 to 18). The median number of months since the last known vaccination dates within our cohort is 7 months (IQR 4 to 9). All participants are part of the COVID-19 contact study, to monitor anti-SARS-CoV-2 immune responses in healthcare workers at the Hannover Medical School (MHH). All participants donated blood directly prior to vaccination with 30µg of the updated BNT162b2 Omicron XBB.1.5 vaccine (Raxtozinameran, BioNTech, Mainz, Germany) in September 2023 and followed up for another blood collection two weeks post vaccination (33). Plasma was separated from collected blood and stored at -80 °C for long term storage and 4°C for immediate use. Detailed information is provided in Supplementary table1.

Statistical analysis

Statistical analysis was performed using GraphPad Prism 9.0 (GraphPad software). Neutralization titers were plotted as geometric mean titers. Data distribution was tested by Shapiro-Wilks. A paired non-parametric Friedman test was performed for non-normally distributed data. In normally distributed data, paired T-tests were performed. P values less than 0.05 were considered significant ns, $p > 0.05$; *, $p \leq 0.05$; **, $p \leq 0.01$; ***, $p \leq 0.001$).

411 **FIGURES AND LEGENDS**

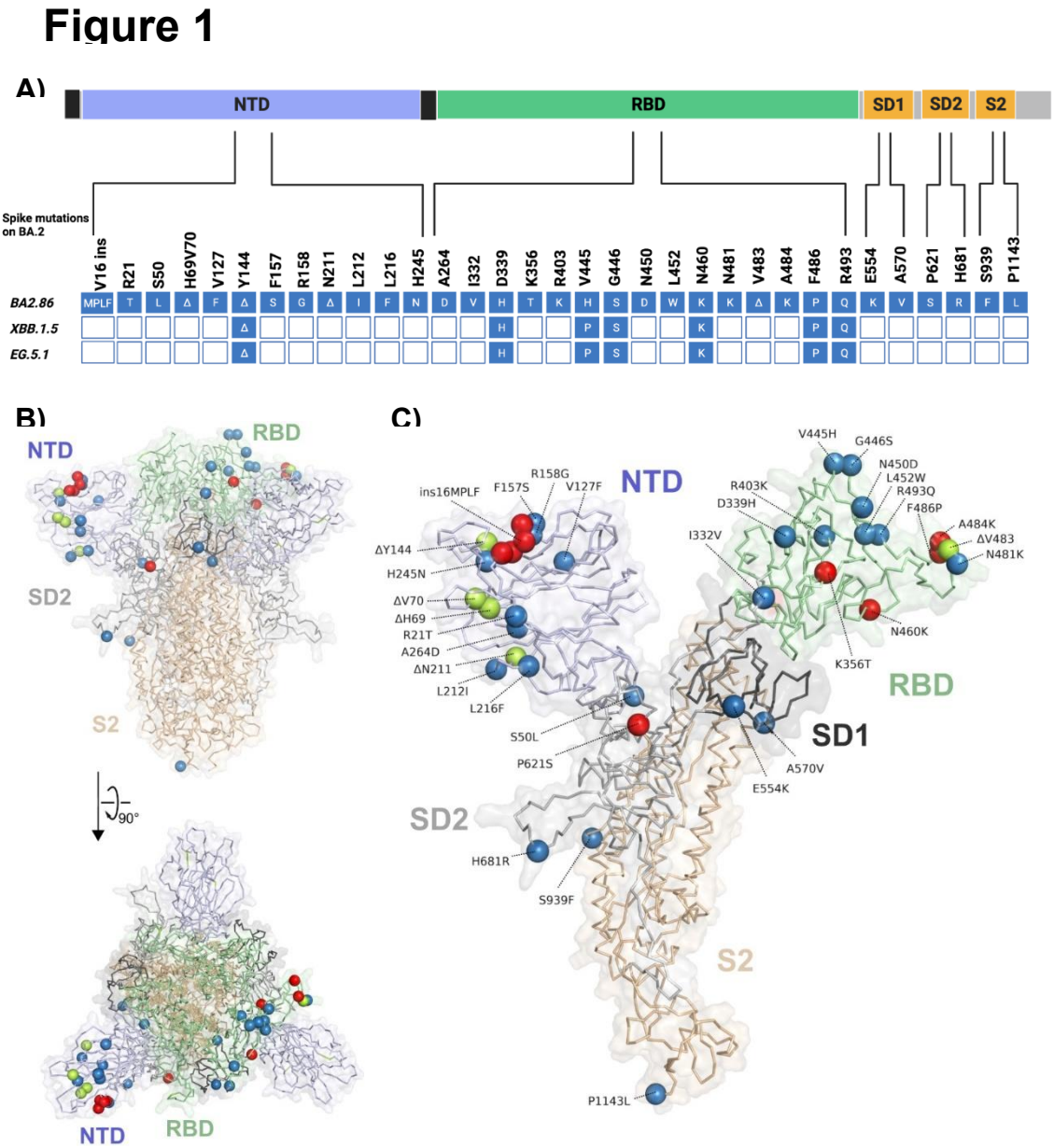

412
413

414 **Figure 1. Overview of BA.2.86 lineage specific spike protein mutations relative to BA.2**

415 (A) Schematic representation of the SARS-CoV-2 spike domains and amino acid changes
416 indicated for BA.2.86, and shared by XBB.1.5, and EG.5.1 compared to the spike of BA.2. N-
417 terminal domain (NTD, blue), receptor binding domain (RBD, green), Subdomains 1 and 2
418 (SD1 and SD2, orange), S2 subunit (orange). (B) Model of the trimeric spike protein of
419 BA.2.86, calculated with AlphaFold2/AlphaFold-Multimer (27, 44). The N-terminal secretion

signal (15 residues) and the C-terminal membrane-anchoring sequence (112 residues) were omitted from calculations, leading to 3372 residues in the final model. Domains have been colored according to panel (A), and one of five independently calculated models is shown. Spheres represent the location of mutations with respect to the spike protein of BA.2. The positions of deletions are colored in green, red spheres indicate mutations that lead to enhanced immune escape of BA.2.86, other mutations are shown in blue. For clarity, mutations are only shown in one chain of the spike trimer. (C) Magnified view of one trimer extracted from the model shown in (B) and shown in the same orientation.

Figure 2

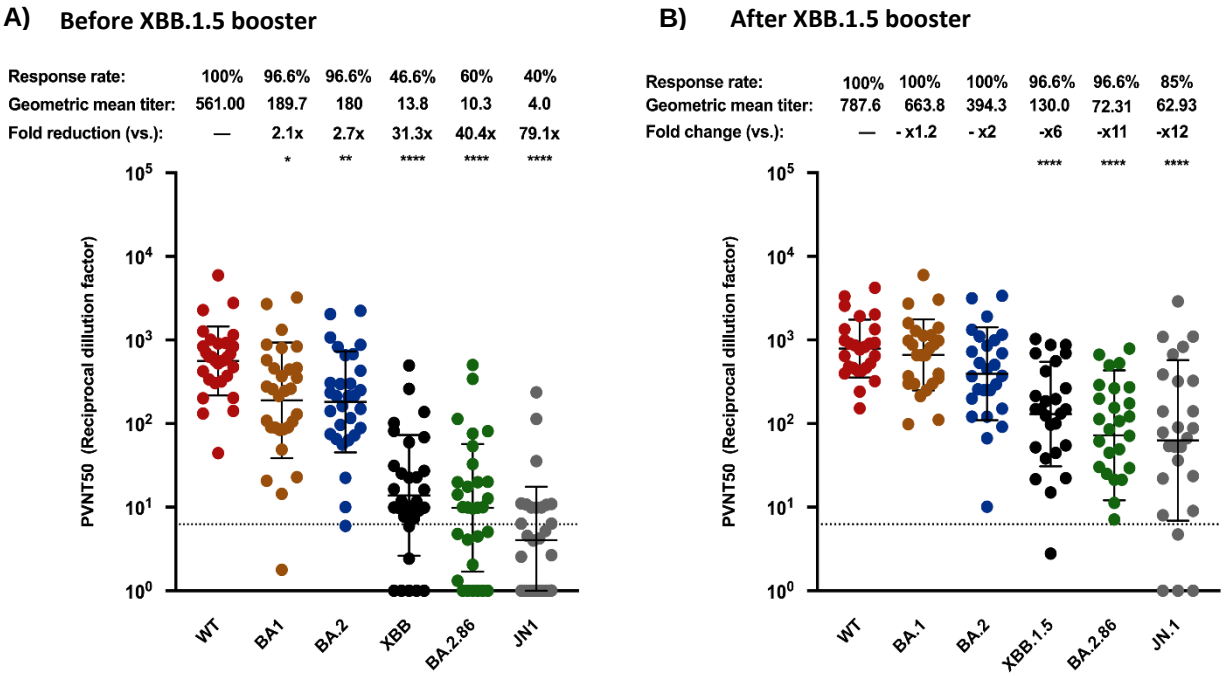

Figure 2. BA.2.86 and JN.1 efficiently evade neutralization in double boostered individuals, but the adapted XBB.1.5 vaccine booster enhances protection against both. (A) Particles pseudo-typed with the indicated S proteins were pre-incubated for one hour at 37 °C with sera dilutions from double boostered health care workers (n=30) (2A) or with plasma dilutions following vaccination with an adapted XBB.1.5 booster (n=26) (2B). Pseudo-

435 virus neutralization titer 50 (PVNT50) was calculated using the least squares fit using a variable
436 slope, using a four-parameter nonlinear regression model and values were plotted as geometric
437 mean. Geometric mean standard deviation bars are shown in black. The lower limit of
438 confidence (LLOC) was set at a PVNT50 of 6.25 (dashed line). Non responders are defined as
439 individuals below this threshold. All PVNT50 below 1 are set at 1 for visualization purposes.
440 The assay was performed in technical duplicates and with negative controls to assess the virus
441 input of each used pseudo-virus in the absence of plasma antibodies. Percentage of positive
442 responders, geometric means, and fold change neutralization over WT-Wuhan$_{pp}$ are shown on
443 top. Friedman nonparametric paired test (ns, $p > 0.05$; *, $p \leq 0.05$; **, $p \leq 0.01$; ***, $p \leq 0.001$).
444 Percentage of positive responders, geometric means, and fold change neutralization over WT-
445 Wuhan$_{pp}$ are shown on top.
446

Figure 3

Neutralisation titers for NTD specific BA.2.86pp mutants pre XBB.1.5 adapted vaccine

A)

Geometric mean titer:	180	10.3	44.9	10.72	5.3	9.5	10	8.2	8.7	13.2	11.2	12.7	17.4	12.2	9.97
Fold change (vs.):	—	-18	-4.0	-17	-34	-19	-18	-22	-21	-14	-16	-14	-10	-15	-18
Sample number:	30	30	20	25	25	18	21	19	20	20	20	21	20	20	23

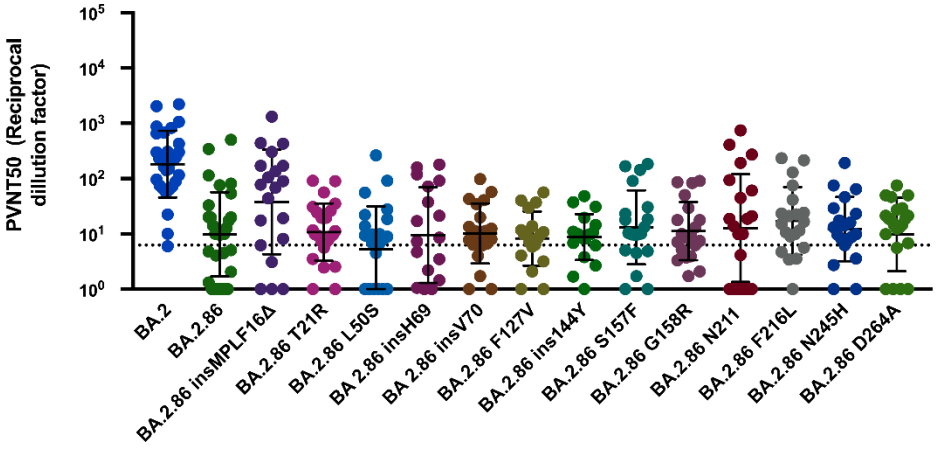

B)

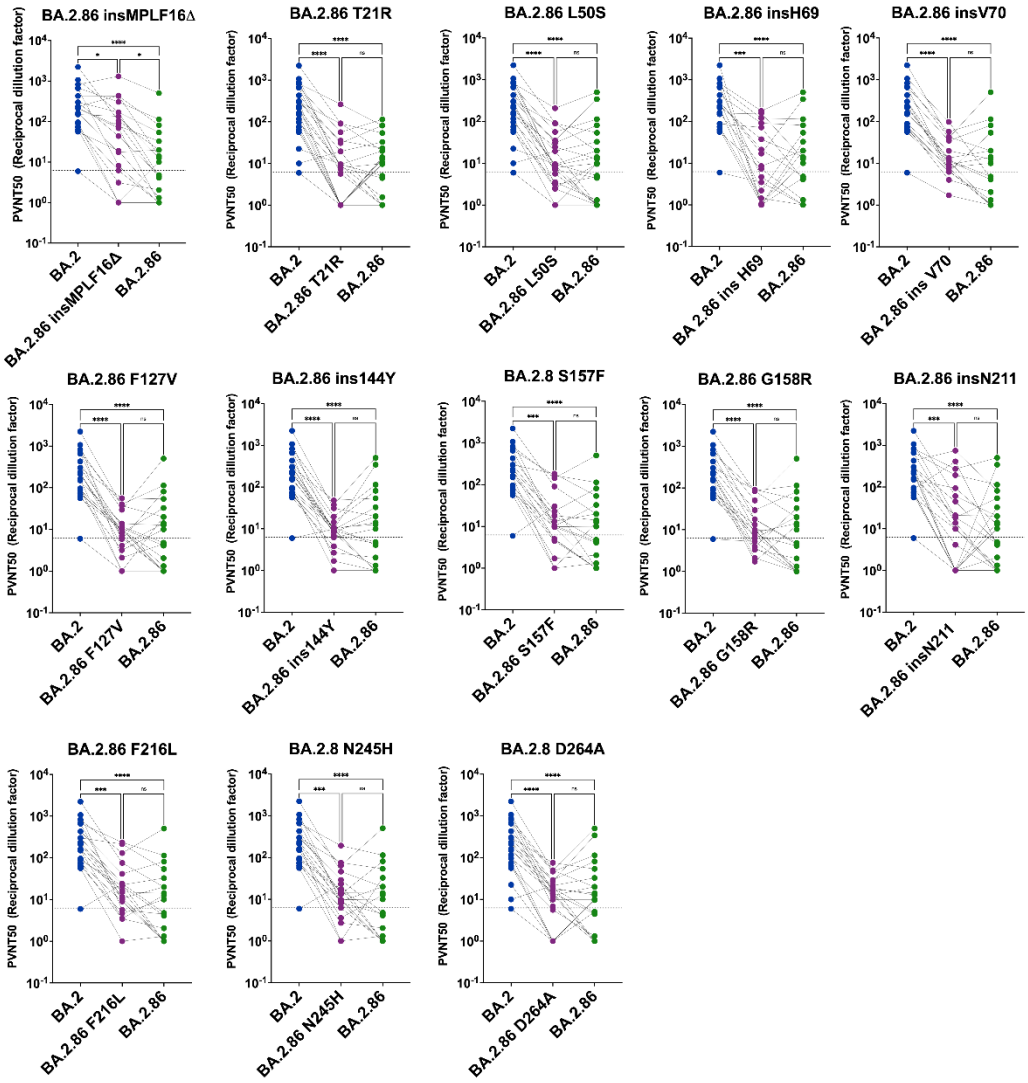

Figure 3. Mapping mutations in the NTD for effects of neutralization efficiency of BA.2.86 in double boostered individuals

(A) Neutralization assessment for particles pseudo-typed with mutations within the NTD of BA.2.86. Each mutant shown contains a single mutation reverting the amino acid mutation in BA.2.86 to the corresponding amino acid within BA.2. Particles pseudo-typed with the indicated S proteins were preincubated for one hour at 37 °C with sera dilutions from double boostered health care workers with non-adapted immunogens. Pseudo-virus neutralization titer 50 (PVNT50) was calculated using the least squares fit using a variable slope, using a four-parameter nonlinear regression model. The lower limit of confidence (LLOC) was set at a PVNT50 of 6.25 (dashed line). Non responders are defined as individuals below this threshold. All PVNT50 below 1 are set at 1 for visualization purposes. The assay was performed in technical duplicates and with negative controls to assess the virus input of each used pseudo-virus in the absence of plasma antibodies. Percentage of positive responders, geometric means, and fold change neutralization over WT-Wuhan$_{pp}$ are shown on top. Geometric mean standard deviation bars are shown in black. (B) Individual neutralization data for particles pseudo-typed with mutations within the NTD of BA.2.86. Statistical significance was assessed by Friedman nonparametric paired test (ns, $p > 0.05$; *, $p \leq 0.05$; **, $p \leq 0.01$; ***, $p \leq 0.001$).

Figure 4

A) **Neutralisation titers for RBD specific BA.2.86pp mutants pre XBB.1.5 adapted vaccine**

Geometric mean titer:	180	10.3	6.7	9.2	28.0	7.6	9.2	9.6	10.6	10.7	26.3	12.3	22.8	23.0	18.6	4.6
Fold reduction (vs.):	—	18x	27x	20x	6x	24x	20x	19x	17x	17x	7x	15x	8x	8x	10x	39x
Sample number:	30	30	25	20	20	19	20	15	20	19	20	21	17	18	20	20

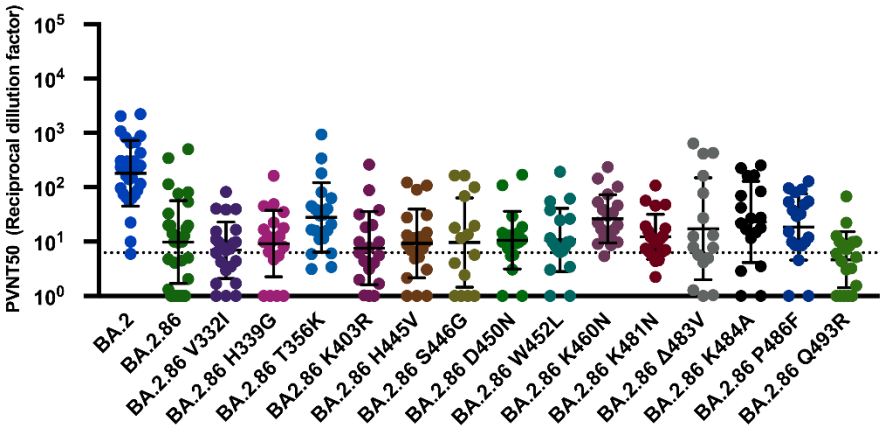

B)

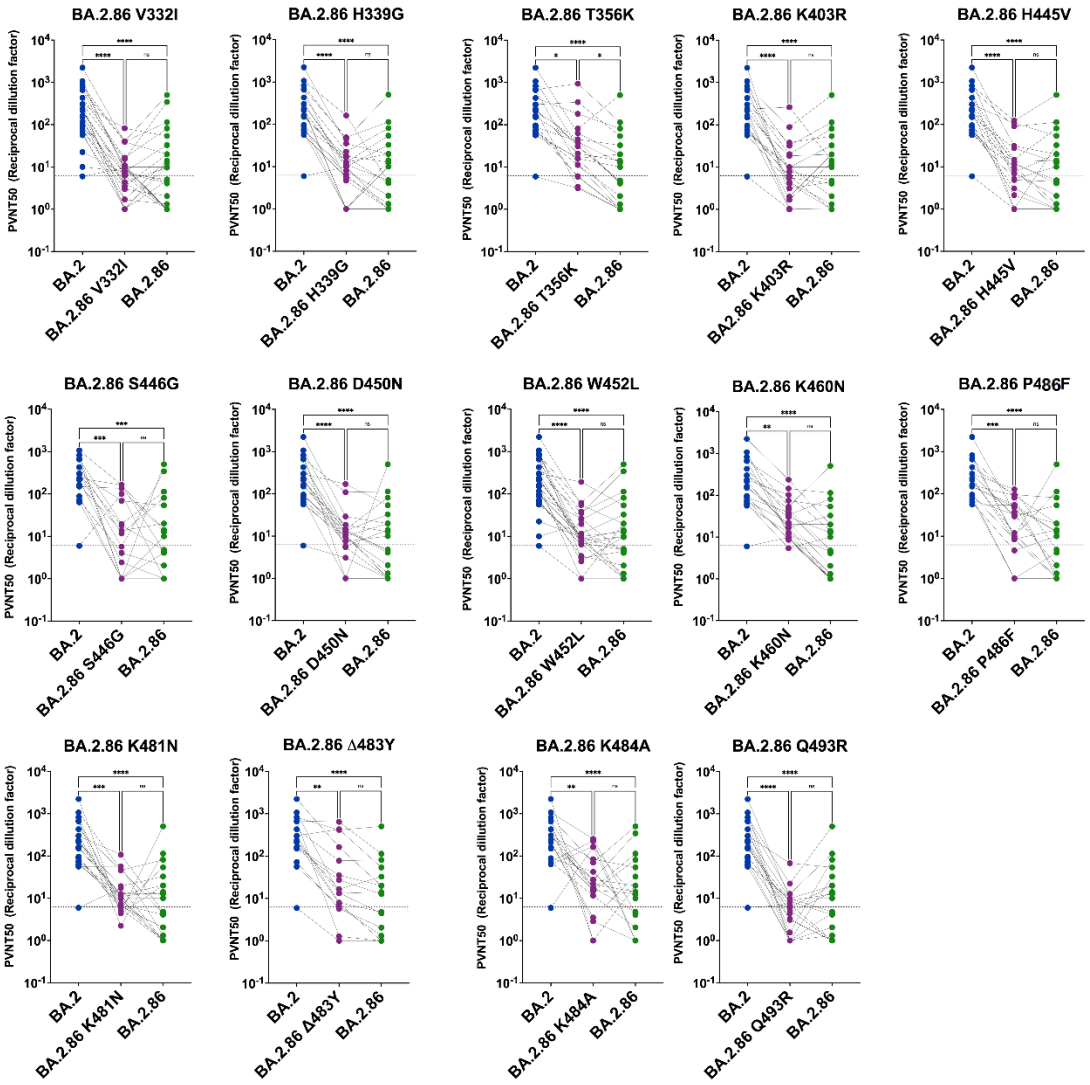

Figure 4. Mutation K356T and to lesser extent K460N, ΔV483, K484A, and P486F within the RBD enhance neutralization efficiency of BA.2.86 in double boostered individuals

(A) Neutralization assessment for particles pseudo-typed with mutations within the RBD of BA.2.86. Each mutant shown contains a single mutation reverting the amino acid mutation in BA.2.86 to the corresponding amino acid within BA.2. Particles pseudo-typed with the indicated S proteins were pre-incubated with serum dilutions from immunized health care workers for one hour at 37 °C. Pseudo-virus neutralization titer 50 (PVNT50) was calculated using the least squares fit using a variable slope, using a four-parameter nonlinear regression model. The lower limit of confidence (LLOC) was set at a PVNT50 of 6.25 (dashed line). Non responders are defined as individuals below this threshold. All PVNT50 below 1 are set at 1 for visualization purposes. The assay was performed in technical duplicates and with negative controls to assess the virus input of each used pseudo-virus in the absence of plasma antibodies. Percentage of positive responders, geometric means, and fold change neutralization over $BA.2_{pp}$ are shown on top. Geometric mean standard deviation bars are shown in black. (B) Individual neutralization data for particles pseudo-typed with mutations within the RBD of BA.2.86. Statistical significance was assessed by Friedman nonparametric paired test (ns, $p > 0.05$; *, $p \leq 0.05$; **, $p \leq 0.01$; ***, $p \leq 0.001$).

Figure 5

Neutralisation titers for S1/S2 and S2 specific BA.2.86pp mutants pre XBB.1.5

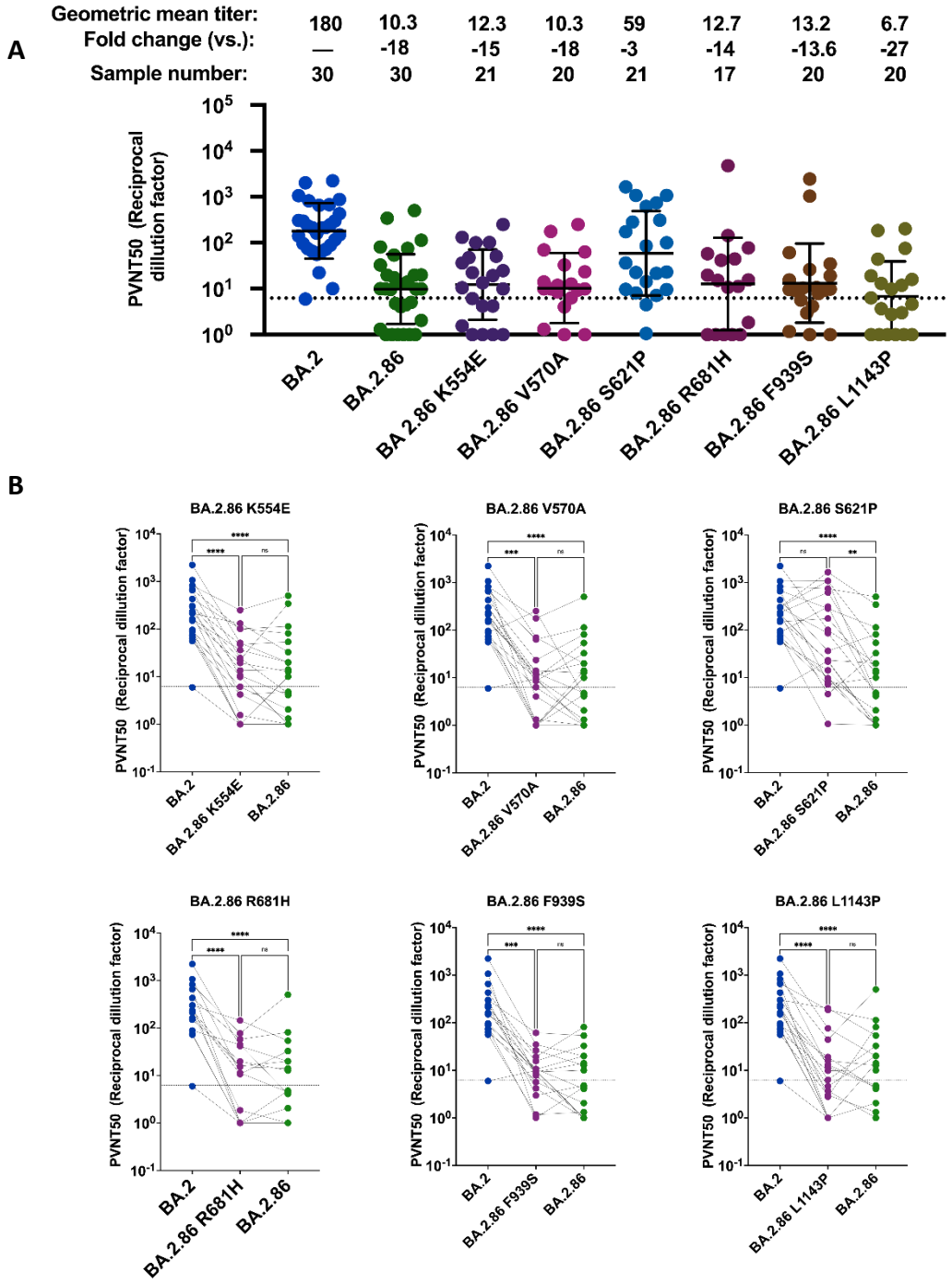

485

486 **Figure 5. Mutation S621P within the S1/S2 domain enhances neutralization efficiency of**

487 **BA.2.86 in double boostered immunized individuals**

488 (A) Neutralization assessment for particles pseudo-typed with mutations within the S1/S2 and

489 S2 domain of BA.2.86. Each mutant shown contains a single mutation reverting the amino acid

mutation in BA.2.86 to the corresponding amino acid within BA.2. Particles pseudo-typed with the indicated S proteins were preincubated for one hour at 37 °C with sera dilutions from double boostered health care workers with non-adapted immunogens. Pseudo-virus neutralization titer 50 (PVNT50) was calculated using the least squares fit using a variable slope, using a four-parameter nonlinear regression model. The lower limit of confidence (LLOC) was set at a PVNT50 of 6.25 (dashed line). Non responders are defined as individuals below this threshold. All PVNT50 below 1 are set at 1 for visualization purposes. The assay was performed in technical duplicates and with negative controls to assess the virus input of each used pseudo-virus in the absence of plasma antibodies. Percentage of positive responders, geometric means, and fold change neutralization over $BA.2_{pp}$ are shown on top. Geometric mean standard deviation bars are shown in black. (B) Individual neutralization data for particles pseudo-typed with mutations within the S1/S2 and S2 domain of BA.2.86. Statistical significance was assessed by Friedman nonparametric paired test (ns, $p > 0.05$; *, $p \leq 0.05$; **, $p \leq 0.01$; ***, $p \leq 0.001$).

Figure 6

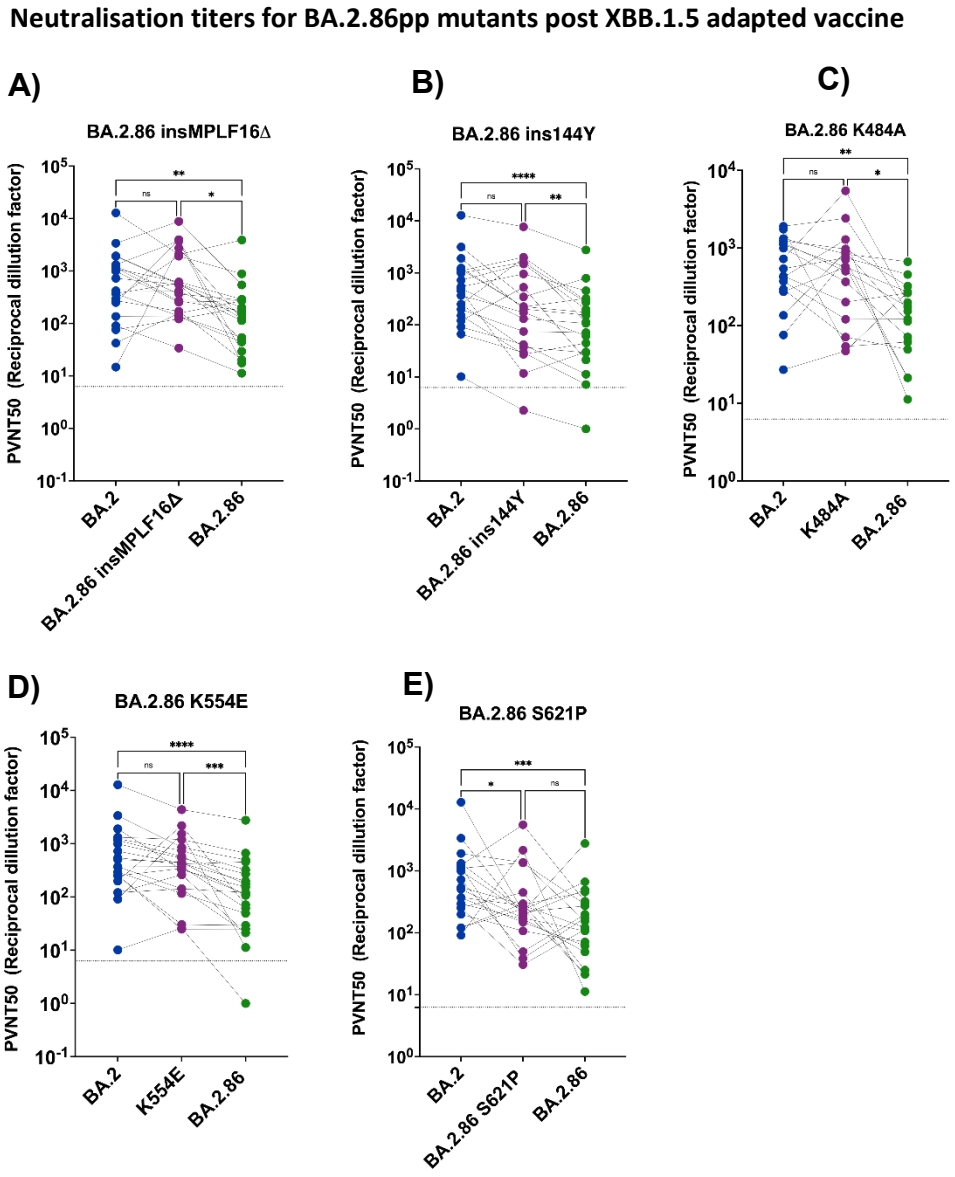

Figure 6: Introduced mutations ΔinsMPLF and Δ144Y within BA.2.86 restores neutralization capacity of sera post BNT162b2 XBB.1.5 vaccination to that of BA.2.

(A-E) Neutralization assessment for pseudo-typed particles with sera post BNT162b2 XBB.1.5 vaccination. Each mutant shown contains a single mutation reverting the amino acid mutation in BA.2.86 to the corresponding amino acid within BA.2. Particles pseudo-typed with the indicated S proteins were pre-incubated for one hour at 37 °C with sera dilutions from double boostered health care workers. Pseudo-virus neutralization titer 50 (PVNT50) was calculated

using the least squares fit using a variable slope, using a four-parameter nonlinear regression model. The lower limit of confidence (LLOC) was set at a PVNT50 of 6.25 (dashed line). Non-responders are defined as individuals below this threshold. All PVNT50 below 1 are set at 1 for visualization purposes. The assay was performed in technical duplicates and with negative controls to assess the virus input of each used pseudo-virus in the absence of plasma antibodies. Statistical significance was assessed by Friedman nonparametric paired test (ns, $p > 0.05$; *, $p \leq 0.05$; **, $p \leq 0.01$; ***, $p \leq 0.001$).

References

1. Callaway E. Why a highly mutated coronavirus variant has scientists on alert. Nature. 2023;620(7976):934.
2. Focosi D, Spezia PG, Maggi F. SARS-CoV-2 BA.2.86 ("Pirola"): Is it Pi or Just Another Omicron Sublineage? Vaccines (Basel). 2023;11(11).
3. Harris E. CDC Assesses Risk From BA.2.86, Highly Mutated COVID-19 Variant. Jama. 2023;330(11):1029.
4. Rasmussen M, Møller FT, Gunalan V, Baig S, Bennedbæk M, Christiansen LE, et al. First cases of SARS-CoV-2 BA.2.86 in Denmark, 2023. Euro Surveill. 2023;28(36).
5. Wannigama DL, Amarasiri M, Phattharapornjaroen P, Hurst C, Modchang C, Chadsuthi S, et al. Tracing the new SARS-CoV-2 variant BA.2.86 in the community through wastewater surveillance in Bangkok, Thailand. Lancet Infect Dis. 2023;23(11):e464-e6.
6. Lambrou AS, South E, Ballou ES, Paden CR, Fuller JA, Bart SM, et al. Early Detection and Surveillance of the SARS-CoV-2 Variant BA.2.86 - Worldwide, July-October 2023. MMWR Morb Mortal Wkly Rep. 2023;72(43):1162-7.
7. Reeve L, Tessier E, Trindall A, Abdul Aziz NIB, Andrews N, Futschik M, et al. High attack rate in a large care home outbreak of SARS-CoV-2 BA.2.86, East of England, August 2023. Euro Surveill. 2023;28(39).
8. Hoffmann M, Kleine-Weber H, Schroeder S, Krüger N, Herrler T, Erichsen S, et al. SARS-CoV-2 Cell Entry Depends on ACE2 and TMPRSS2 and Is Blocked by a Clinically Proven Protease Inhibitor. Cell. 2020;181(2):271-80.e8.
9. Lusvarghi S, Wang W, Herrup R, Neerukonda SN, Vassell R, Bentley L, et al. Key Substitutions in the Spike Protein of SARS-CoV-2 Variants Can Predict Resistance to Monoclonal Antibodies, but Other Substitutions Can Modify the Effects. J Virol. 2022;96(1):e0111021.
10. Zhou P, Yang XL, Wang XG, Hu B, Zhang L, Zhang W, et al. A pneumonia outbreak associated with a new coronavirus of probable bat origin. Nature. 2020;579(7798):270-3.
11. Yang S, Yu Y, Jian F, Song W, Yisimayi A, Chen X, et al. Antigenicity and infectivity characterisation of SARS-CoV-2 BA.2.86. Lancet Infect Dis. 2023;23(11):e457-e9.
12. Uriu K, Ito J, Kosugi Y, Tanaka YL, Mugita Y, Guo Z, et al. Transmissibility, infectivity, and immune evasion of the SARS-CoV-2 BA.2.86 variant. Lancet Infect Dis. 2023;23(11):e460-e1.
13. Wang Q, Guo Y, Liu L, Schwanz LT, Li Z, Nair MS, et al. Antigenicity and receptor affinity of SARS-CoV-2 BA.2.86 spike. Nature. 2023.
14. Qian W, Yicheng G, Anthony B, Ian AM, Riccardo V, Carmen G, et al. XBB.1.5 monovalent mRNA vaccine booster elicits robust neutralizing antibodies against emerging SARS-CoV-2 variants. bioRxiv. 2023:2023.11.26.568730.
15. Dadonaite B, Brown J, McMahon TE, Farrell AG, Asarnow D, Stewart C, et al. Full-spike deep mutational scanning helps predict the evolutionary success of SARS-CoV-2 clades. bioRxiv. 2023.
16. Pastorio C, Zech F, Noettger S, Jung C, Jacob T, Sanderson T, et al. Determinants of Spike infectivity, processing, and neutralization in SARS-CoV-2 Omicron subvariants BA.1 and BA.2. Cell host & microbe. 2022;30(9):1255-68.e5.
17. Abassi L, Bertoglio F, Mačak Šafranko Ž, Schirrmann T, Greweling-Pils M, Seifert O, et al. Evaluation of the Neutralizing Antibody STE90-C11 against SARS-CoV-2 Delta Infection and Its Recognition of Other Variants of Concerns. Viruses. 2023;15(11).

18. Miller J, Hachmann NP, Collier AY, Lasrado N, Mazurek CR, Patio RC, et al. Substantial Neutralization Escape by SARS-CoV-2 Omicron Variants BQ.1.1 and XBB.1. N Engl J Med. 2023;388(7):662-4.
19. Yue C, Song W, Wang L, Jian F, Chen X, Gao F, et al. ACE2 binding and antibody evasion in enhanced transmissibility of XBB.1.5. Lancet Infect Dis. 2023;23(3):278-80.
20. Wang Q, Guo Y, Iketani S, Nair MS, Li Z, Mohri H, et al. Antibody evasion by SARS-CoV-2 Omicron subvariants BA.2.12.1, BA.4 and BA.5. Nature. 2022;608(7923):603-8.
21. McCallum M, De Marco A, Lempp FA, Tortorici MA, Pinto D, Walls AC, et al. N-terminal domain antigenic mapping reveals a site of vulnerability for SARS-CoV-2. Cell. 2021;184(9):2332-47.e16.
22. Vellas C, Trémeaux P, Del Bello A, Latour J, Jeanne N, Ranger N, et al. Resistance mutations in SARS-CoV-2 omicron variant in patients treated with sotrovimab. Clin Microbiol Infect. 2022;28(9):1297-9.
23. Mykytyn AZ, Fouchier RA, Haagmans BL. Antigenic evolution of SARS coronavirus 2. Curr Opin Virol. 2023;62:101349.
24. Huo J, Dijokaite-Guraliuc A, Liu C, Zhou D, Ginn HM, Das R, et al. A delicate balance between antibody evasion and ACE2 affinity for Omicron BA.2.75. Cell Rep. 2023;42(1):111903.
25. Qu P, Evans JP, Zheng YM, Carlin C, Saif LJ, Oltz EM, et al. Evasion of neutralizing antibody responses by the SARS-CoV-2 BA.2.75 variant. Cell Host Microbe. 2022;30(11):1518-26.e4.
26. Tunyasuvunakool K, Adler J, Wu Z, Green T, Zielinski M, Žídek A, et al. Highly accurate protein structure prediction for the human proteome. Nature. 2021;596(7873):590-6.
27. Richard E, Michael ON, Alexander P, Natasha A, Andrew S, Tim G, et al. Protein complex prediction with AlphaFold-Multimer. bioRxiv. 2022:2021.10.04.463034.
28. Yuan Y, Cao D, Zhang Y, Ma J, Qi J, Wang Q, et al. Cryo-EM structures of MERS-CoV and SARS-CoV spike glycoproteins reveal the dynamic receptor binding domains. Nature communications. 2017;8:15092.
29. Katzmarzyk M, Clesle DC, van den Heuvel J, Hoffmann M, Garritsen H, Pöhlmann S, et al. Systematical assessment of the impact of single spike mutations of SARS-CoV-2 Omicron sub-variants on the neutralization capacity of post-vaccination sera. Front Immunol. 2023;14:1288794.
30. Sheward DJ, Yang Y, Westerberg M, Öling S, Muschiol S, Sato K, et al. Sensitivity of the SARS-CoV-2 BA.2.86 variant to prevailing neutralising antibody responses. Lancet Infect Dis. 2023;23(11):e462-e3.
31. Berkhout B, Herrera-Carrillo E. SARS-CoV-2 Evolution: On the Sudden Appearance of the Omicron Variant. J Virol. 2022;96(7):e0009022.
32. Raglow Z, Surie D, Chappell JD, Zhu Y, Martin ET, Kwon JH, et al. SARS-CoV-2 shedding and evolution in immunocompromised hosts during the Omicron period: a multicenter prospective analysis. medRxiv. 2023.
33. Stankov MV, Hoffmann M, Gutierrez Jauregui R, Cossmann A, Morillas Ramos G, Graalmann T, et al. Humoral and cellular immune responses following BNT162b2 XBB.1.5 vaccination. Lancet Infect Dis. 2023.
34. Chi X, Yan R, Zhang J, Zhang G, Zhang Y, Hao M, et al. A neutralizing human antibody binds to the N-terminal domain of the Spike protein of SARS-CoV-2. Science (New York, NY). 2020;369(6504):650-5.
35. Suryadevara N, Shiakolas AR, VanBlargan LA, Binshtein E, Chen RE, Case JB, et al. An antibody targeting the N-terminal domain of SARS-CoV-2 disrupts the spike trimer. J Clin Invest. 2022;132(11).

618 36. Colson P, La Scola B, Beye M, Delerce J, Raoult D, Fantini J. Emergence of a second
619 SARS-CoV-2 variant with a tremendous genetic leap from its ancestors. J Med Virol.
620 2023;95(10):e29124.
621 37. Wang Q, Li Z, Guo Y, Mellis IA, Iketani S, Liu M, et al. Evolving antibody evasion
622 and receptor affinity of the Omicron BA.2.75 sublineage of SARS-CoV-2. iScience.
623 2023;26(11):108254.
624 38. Wang Q, Iketani S, Li Z, Liu L, Guo Y, Huang Y, et al. Alarming antibody evasion
625 properties of rising SARS-CoV-2 BQ and XBB subvariants. Cell. 2023;186(2):279-86.e8.
626 39. Wang Q, Iketani S, Li Z, Guo Y, Yeh AY, Liu M, et al. Antigenic characterization of
627 the SARS-CoV-2 Omicron subvariant BA.2.75. Cell Host Microbe. 2022;30(11):1512-7.e4.
628 40. Lester S, Harcourt J, Whitt M, Al-Abdely HM, Midgley CM, Alkhamis AM, et al.
629 Middle East respiratory coronavirus (MERS-CoV) spike (S) protein vesicular stomatitis virus
630 pseudoparticle neutralization assays offer a reliable alternative to the conventional
631 neutralization assay in human seroepidemiological studies. Access Microbiol.
632 2019;1(9):e000057.
633 41. Tolah AMK, Sohrab SS, Tolah KMK, Hassan AM, El-Kafrawy SA, Azhar EI.
634 Evaluation of a Pseudovirus Neutralization Assay for SARS-CoV-2 and Correlation with
635 Live Virus-Based Micro Neutralization Assay. Diagnostics (Basel). 2021;11(6).
636 42. Quandt J, Muik A, Salisch N, Lui BG, Lutz S, Krüger K, et al. Omicron BA.1
637 breakthrough infection drives cross-variant neutralization and memory B cell formation
638 against conserved epitopes. Sci Immunol. 2022;7(75):eabq2427.
639 43. Berger Rentsch M, Zimmer G. A vesicular stomatitis virus replicon-based bioassay
640 for the rapid and sensitive determination of multi-species type I interferon. PLoS One.
641 2011;6(10):e25858.
642 44. Jumper J, Evans R, Pritzel A, Green T, Figurnov M, Ronneberger O, et al. Highly
643 accurate protein structure prediction with AlphaFold. Nature. 2021;596(7873):583-9.
644

645

SUPPLEMENTARY INFORMATION

Table S1: Detailed information on the plasma samples.

Figure S1. Analysis of the structural model of the BA.2.86 spike protein

(A) AlphaFold2/AlphaFold-Multimer model of the trimeric spike protein, colored by per-residue model confidence score (pLDDT), with blue colors corresponding to high and red colors corresponding to low confidence. The circle highlights the N-terminal domain NTD further explored in the next panel. (B) The NTD of BA.2.86 spike protein colored by pLDDT score. The circle highlights the N-terminal 16MPLF insertion of BA.2.86 and is further explored in the next panel. (C) Predicted interactions of the 16MPLF insertion with a crevice of the NTD. Colors correspond to the pLDDT score, N marks the position of the N-terminus after cleavage of the signal peptide. (D) Comparison to the same region in the NTD of SARS-CoV (PDB-ID 5X4S) (28). Note that this virus, with respect to SARS-CoV-2, carried an extended N-terminus as well. Here, the N-terminus was anchored by a disulfide bridge (C19-C133), which is not conserved in BA.2.86.